13th National Congress on Civil Engineering
10 & 11, May 2022
Isfahan University of Technology, Isfahan, Iran

Sentinel-2 Band Selection for Water Quality Parameters Measurement in the Gorgan Gulf

Reza Mofidi Neyestani[1], Massoud Tajrishy[2*]
Department of Civil Engineering, Sharif University of Technology, Azadi Avenue, Tehran, Iran
⋮
Tajrishy@sharif.edu

Abstract

Surface water quality management needs water contaminants monitoring and information about water quality parameters. Field measurement is a costly, time-consuming procedure that limits information about the whole surface of a water body. Remote sensing methods are valuable ways that prepare water quality information using different characteristics between reflectance detected from each parameter. However, there are some limitations to choosing and classifying satellite bands for various parameters. This article discusses the Sentinel-2 band selection to measure water quality parameters in the Gorgan Gulf. Considering different bands for extracting an approximate quantity of Total Dissolved Solids, Salinity, Electrical Conductivity, Chlorophyll-a, and Turbidity, a Bayesian Linear Regression model has been used for detecting the correlation between different Sentinel-2 bands and field measurements on two dates with a one-year interval. The result declares that using all of the Sentinel-2 bands to increase the accuracy of the quantitative results is not a reliable choice. Even if some predictions' accuracy seems rational, spectral signatures should be considered to extract dependable equations for water quality measurements utilizing remote sensing.

Keywords: Gorgan Gulf, Surface Water Quality, Remote Sensing, Sentinel-2, Bayesian Regression.

1. INTRODUCTION

More than half of the world's population lives near surface waters, and their activities cause increasing water contaminants[1]. Anthropogenic effects on surface waters include intentional or accidental discharge of domestic, industrial, and municipal wastewater and the use of chemical pesticides in drained agricultural lands[2]. Water pollution by anthropogenic activities leads to various harmful effects like threatening human health, preventing marine activities such as fishing, and disrupting water quality to use in various applications[3]. Among surface water resources, gulfs' water quality is more important because its contaminants can threaten the health of terrestrial and aquatic organisms by creating a dead zone[4, 5]. Accordingly, surface water quality monitoring is a critical feature that facilitates managing water resources, detecting contaminants, and controlling their harmful effects on human health. Decision-makers also can use these data to conduct protection programs and policies.

Water quality parameters measurement could be done using traditional methods (boats and portable sensors), but these methods are expensive and time-consuming[6]. In addition, these methods are point-based and could measure and extract water quality parameters only on limited points. Due to point sampling in traditional methods, to predict values at points where measurements have not been made, it is necessary to interpolate. As a result, some errors would occur in predictions. Nowadays, satellite remote sensing techniques are among the best alternatives to traditional water quality measurements [7]. Although using remote sensing techniques to measure water quality parameters is an approximate method, it provides wide coverage[8], reduced costs[9], increased measurement speed and accuracy[1], and reduced labor requirements[10]. Various parameters such as Total Suspended Solids (TDS)[11], Colored Dissolved Organic Matter (CDOM)[12], Chlorophyll-a (Chl-a)[13], Salinity[14], Electrical Conductivity (EC) [15], Turbidity[16] and Sea Surface Temperature (SST)[17] can be measured using remote sensing.

Remote sensing for water quality parameters estimation has two key factors. The first is the algorithm used to detect the relationship between reflectance from different spectral bands of the satellite, and the second is the band selection for every parameter. Different Machine Learning (ML) algorithms[18] and other statistical algorithms such as Regression[19] have been used to find the relation between satellite bands' reflectance and field measurements. Some algorithms, such as regression, are based on weighting input spectral bands. Others, such as Artificial Neural Network (ANN) algorithms, are black boxes that do not need physical pre-

information; in these methods, all bands enter the model, and the model decides which are more correlated to the target parameter.
In this article, Bayesian Linear Regression (BLR) has been used to detect the relationship between Gorgan Gulf field measurements of TDS, Salinity, EC, Chl-a, and Turbidity and reflectance values provided from Sentinel-2 spectral bands. To recognize the best band selection, two dates field measurement correlation with Sentinel-2 two sets of bands reflectance values have been compared. The final surface water quality map of each parameter has been exported for the best band combination. The study's primary goal is to indicate the effect of two sets of Sentinel-2 spectral bands on the water quality parameters' prediction accuracy. This study also aims to evaluate the BLR model's capability to predict the Gorgan Gulf water quality parameters.

2. STUDY AREA

Gorgan Gulf (Figure 1), the largest gulf in the Caspian Sea with a maximum depth of 4 meters, is home to a variety of aquatic species. This gulf is located in the southeast of the Caspian Sea within longitude of 53°34'56.351"E to 54°2'34.634"E and latitude of 36°46'40.287"N to 36°56'13.326"N. The Gorgan Gulf area extracted by Sentinel-2 imagery on 11 September 2020 was 377 square kilometers and has been decreased to 355 square kilometers at 28 June 2021. The maximum water depth of the gulf is located near the southern side of Ashuradeh and decreases from east to west, but in general, the gulf is one of the shallow water sources. Cities around the gulf whose sewage disposal directly affects the pollution of the bay water are Bandar-e-Gaz, Bandar-e-Turkmen, Gomishan, and Kordkoy.

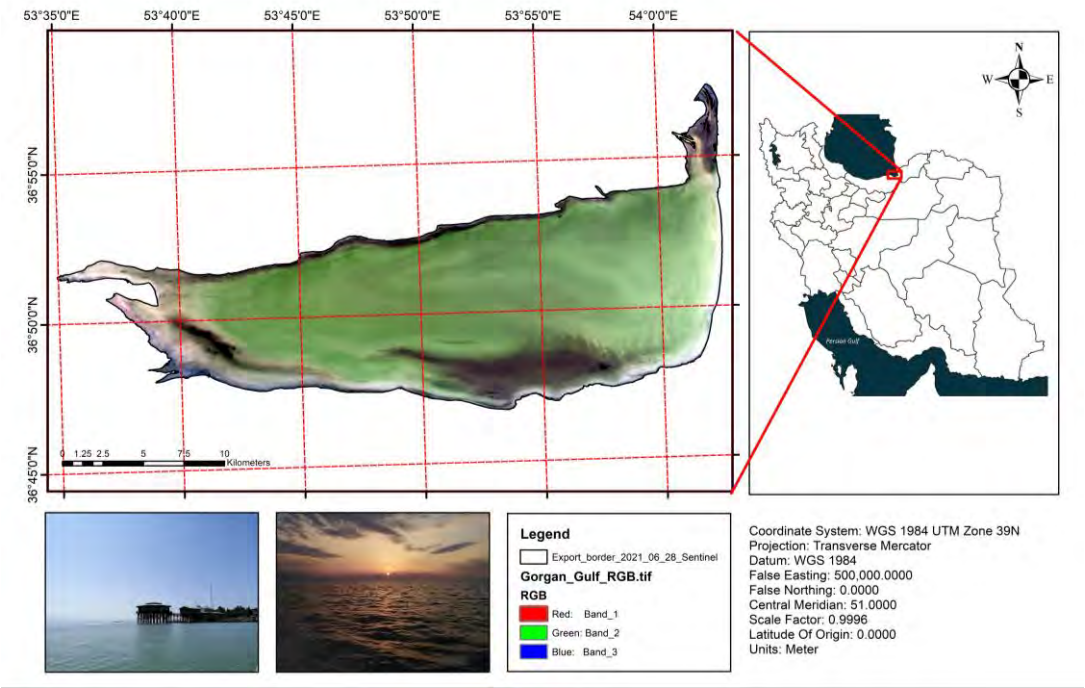

Figure 1: Gorgan Gulf location and area at 28 June 2021.

3. METHOD

3.1. Data

3.1.1. Satellite Data

The Sentinel-2 mission provides high-resolution, multi-spectral images to use in different fields of study. Sentinel-2 Multispectral Imagery (MSI) data has 13 spectral bands ranging from visible to short wave infrared (SWIR) spectral region with a high spectral resolution (10m to 60m) and a radiometric quantization of 12-bit[16]. Bands' information is provided in Table 1. The satellite images of two dates (11 September 2020 and 28 June 2021) were downloaded using Google Earth Engine (GEE). Also, all of the computational processes on satellite images were done utilizing GEE.

Table 1: Sentinel-2 bands in the range of visible to SWIR spectral region[20].

Name	Resolution	Wavelength	Description
B1	60 meters	443.9nm (S2A) / 442.3nm (S2B)	Aerosols
B2	10 meters	496.6nm (S2A) / 492.1nm (S2B)	Blue
B3	10 meters	560nm (S2A) / 559nm (S2B)	Green
B4	10 meters	664.5nm (S2A) / 665nm (S2B)	Red
B5	20 meters	703.9nm (S2A) / 703.8nm (S2B)	Red Edge 1
B6	20 meters	740.2nm (S2A) / 739.1nm (S2B)	Red Edge 2
B7	20 meters	782.5nm (S2A) / 779.7nm (S2B)	Red Edge 3
B8	10 meters	835.1nm (S2A) / 833nm (S2B)	Near-Infrared (NIR)
B8A	20 meters	864.8nm (S2A) / 864nm (S2B)	Red Edge 4
B9	60 meters	945nm (S2A) / 943.2nm (S2B)	Water vapor
B11	20 meters	1613.7nm (S2A) / 1610.4nm (S2B)	SWIR 1
B12	20 meters	2202.4nm (S2A) / 2185.7nm (S2B)	SWIR 2

3.1.2 Field measured Data

Sampling in the Gorgan Gulf was done when the Sentinel-2 satellite was passing above the gulf. Seventy-two stations were sampled using motorboat in two days for each satellite pass date. Among all the stations, thirty-one stations belonged on 11 September 2020, and forty-one were on 28 June 2021. Locations of the stations for each date are displayed in Figure 2. TDS, Salinity, EC, Chl-a, and Turbidity values for each station were measured using field sensors. The computational procedures were done using these values after preprocessing and cleaning from noisy data.

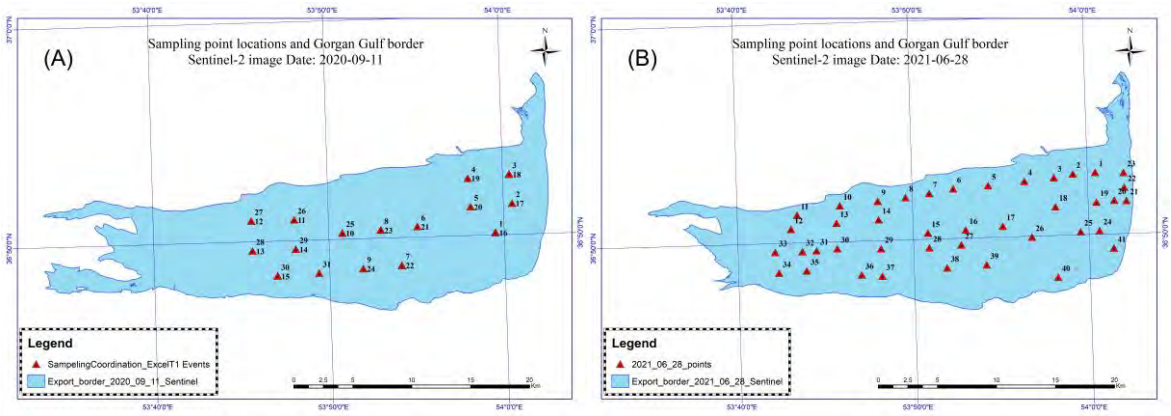

Figure 2: sampling stations at (A) 11 September 2020 and (B) 28 June 2021 with Gorgan Gulf border extracted by Sentinel-2 image at mentioned dates.

3.2. Bayesian Linear Regression (BLR) Model

The basics of BLR are available in [21]. The most important reason the model was chosen was the low computational cost and band selection using the statistical distribution of the predictors. All BLR models were created using the Rtx application[22–24]. Field measured data for each parameter was the dependent variable, and the Sentinel-2 reflectance for each band at the same location of the field measured data was the predictor of the model. Twenty percent of values were separated randomly to test and validate the model for each parameter at each date. At the next steps, parameters with a coefficient of variation of more than 30 percent were eliminated, respectively. This repeated until all model parameters' coefficients of variation became lower than 30, or eliminating them significantly changed the sigma coefficient of variation. In each step, the R-factor value was checked not to be lower than the expectation. All the steps can be followed in Figure 3. After each step, model predictions vs. observation plots are checked and exported. The process was done for all five parameters with two different sets of bands explained in the following parts.

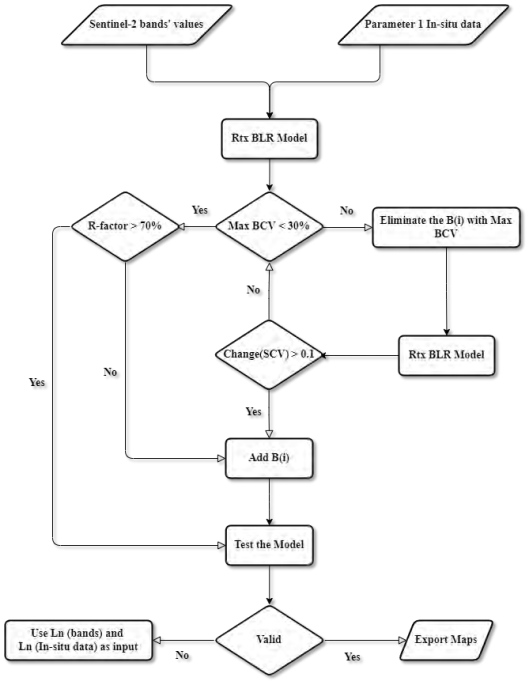

Figure 3: BLR Model flowchart. BCV is the abbreviation of "Bands Coefficient of variation," and SCV is the abbreviation of "Sigma's Coefficient of variation."

3.2.1. BLR Model Using Seven Bands

The BLR model for each date and parameter was made using Sentinel-2 seven bands' reflectance. The bands were: B1(Aerosols), B2(Blue), B3(Green), B4(Red), B8(NIR), B11(SWIR1), B12(SWIR2). Because of these bands' different resolutions (10m to 60m), all of them were aligned with 10m resolution.

3.2.2. BLR Model Using Four Bands

In this part, reflectance values of Sentinel-2 four bands were used for creating the BLR model. The bands were: B2(Blue), B3(Green), B4(Red), B8(NIR), and the model was created for each parameter at both dates. There is no need to change images' resolution because the bands' resolution equal 10m. The model has been made for two main reasons. The first reason is that lowering the number of the input bands to the model reduces computational costs, and the second reason is based on water spectral signature. Both clean water and water with phytoplankton reflectance wavelength are in the range of 0 to 0.8 micrometer[25]. The four selected bands cover the range and simultaneously reduce the number of input bands.

4. RESULTS AND DISCUSSION

4.1. BLR Model Results

The best BLR model's prediction vs. observation plot for all parameters can be followed in **Error! Reference source not found.**. As explained in part 3.2., if the raw input data did not have the minimum expected value for the R-factor, the natural logarithm of the data would be considered to predict parameters' values. Figure 4 indicates that natural logarithm input has been used for seven bands on 11 September 2020 of Salinity, Chl-a, and Turbidity; four bands on 11 September 2020 of TDS, EC, Chl-a, and Turbidity; seven bands and four bands on 28 June 2021 of Chl-a, and Turbidity. Bands selected for each date and the R-factor for each are indicated in Table 2. Based on Figure 4 and Table 2, it could be concluded that natural logarithm input is better for chlorophyll-a and turbidity prediction. According to Table 2, the R-factor of four bands input is lower than that of seven bands input for both dates and all of the parameters. Although R-factor is not the determinant parameter and there are other statistical indexes and values, such as Root-Mean-Square Error (RMSE), that should be compared, it could be concluded the BLR model fit reduces when using four bands as the input.

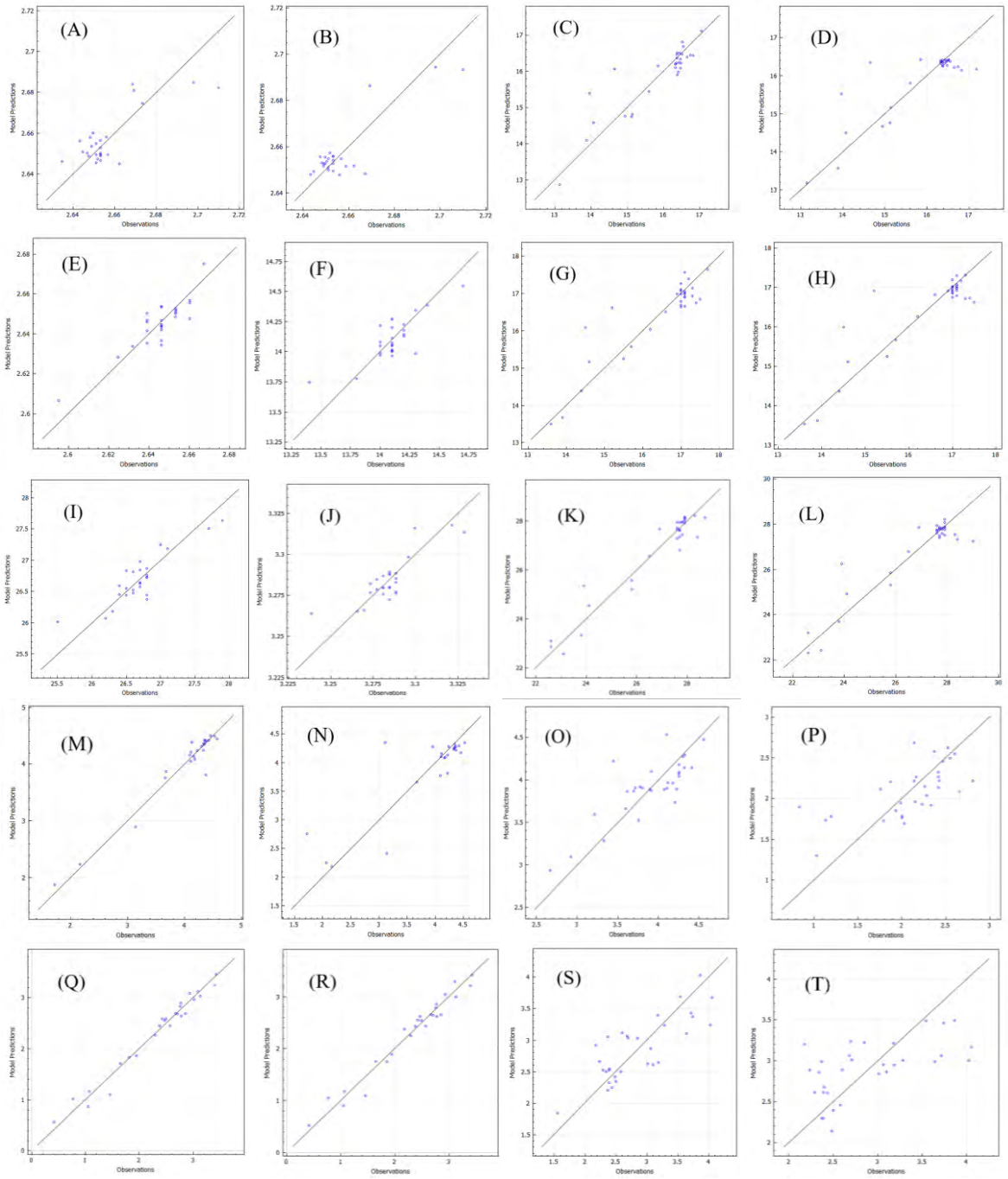

Figure 4: BLR model predictions vs. observation scatter plot for seven bands at 11 September 2020 for (A) TDS, (E) Salinity, (I) EC, (M) Chl-a, and (Q) Turbidity; four bands at 11 September 2020 for (B) TDS, (F) Salinity, (J) EC, (N) Chl-a, and (R) Turbidity; seven bands at 28 June 2021 for (C) TDS, (G) Salinity, (K) EC, (O) Chl-a, and (S) Turbidity; four bands at 28 June 2021 for (D) TDS, (H) Salinity, (L) EC, (P) Chl-a, and (T) Turbidity.

SWIR bands wavelength (1613.7nm to 2202.4nm) are more than water spectral signature, and using them as predictors is not rational. Band-3(Green) is presented in all of the predictors, and the reason is that the peak of the water spectral signature occurs near its wavelength (560nm). Conclusively, the band is one of the best predictors for water quality parameters. Band-1(Aerosols) is affected by atmospheric particles because of its wavelength (444nm). In this regard, this band cannot be chosen as the best band for parameters prediction. Although Band-8(NIR) contains lower reflectance from water than bands with lower wavelengths, it is valuable for vegetation prediction because vegetation spectral signature peak is in the same wavelength range as this band. As a result, Band-8 could be used to detect and approximate chlorophyll-a or other parameters with

vegetation basis in water. Band-2(Blue) and Band-4(Red) are two bands in the range of water spectral signature. These two bands could be helpful in some water quality parameters measurement.

Table 2: selected bands and R-factor for each parameter at each date.

parameter	11 September 2020 Sampling				28 June 2021 Sampling			
	7 Bands		4 Bands		7 Bands		4 Bands	
	Selected bands	R-factor	Selected bands	R-factor	Selected bands	R-factor	Selected bands	R-factor
$TDS\left(\frac{g}{L}\right)$	B2(Blue), B3(Green)	0.7944	B2(Blue), B3(Green)	0.7935	B1, B2(Blue), B4(Red)	0.8889	B2(Blue), B3(Green)	0.8328
$Salinity\ \left(\frac{g}{L}\right)$	B1, B3(Green), B8(NIR), B11(SWIR1), B12(SWIR2)	0.8727	B3(Green), B4(Red), B8(NIR)	0.8013	B1, B2(Blue)	0.9093	B2(Blue)	0.8976
$EC\left(\frac{ms}{cm}\right)$	B3(Green), B4(Red), B8(NIR)	0.8764	B3(Green), B4(Red), B8(NIR)	0.8124	B2(Blue), B4(Red), B11(SWIR1)	0.9639	B2(Blue), B3(Green)	0.9128
$Chl-a\left(\frac{\mu g}{L}\right)$	B2(Blue), B3(Green), B4(Red), B11(SWIR1), B12(SWIR2)	0.9440	B3(Green), B4(Red), B8(NIR)	0.8404	B3(Green), B4(Red), B8(NIR)	0.7978	B3(Green), B4(Red), B8(NIR)	0.7161
$Turbidity\ (NTU)$	B1, B3(Green), B8(NIR)	0.9788	B3(Green), B8(NIR)	0.9725	B1, B4(Red), B8(NIR), B11(SWIR1), B12(SWIR2)	0.7378	B2(Blue), B3(Green), B8(NIR)	0.7370

4.2. Test the Model

In the previous part, the BLR model was created for each date. In this part, two tests are made for the model. At the first step, the model created for each date is tested using 20 percent of the input data (test data) to evaluate the model's validity for the date. At the next step, the model that is created for 11 September 2020 is used to predict the values of the parameters on 28 June 2021. The main purpose of the step is to compare between seven bands input and four bands input and validate the model to predict water quality parameters' values at other dates. RMSE of models for each step is calculated and mentioned in Table 3.

Table 3: The RMSE of models (1) using test data of the model, and (2) predicting the values of the five parameters on 28 June 2021 using the model made for 11 September 2020.

parameter	11 September 2020 Sampling		28 June 2021 Sampling			
	7 Bands	4 Bands	7 Bands		4 Bands	
	RMSE (1)	RMSE (1)	RMSE (1)	RMSE (2)	RMSE (1)	RMSE (2)
$TDS\left(\frac{g}{L}\right)$	0.0081	0.0014	0.0363	0.1138	0.0360	0.1132
$Salinity\ \left(\frac{g}{L}\right)$	0.0182	0.0136	0.0508	0.2601	0.0496	0.2094
$EC\left(\frac{ms}{cm}\right)$	0.1491	0.0107	0.0977	0.2516	0.0972	0.1429
$Chl-a\left(\frac{\mu g}{L}\right)$	0.8070	0.2117	0.2867	0.9278	0.2485	0.9055
$Turbidity\ (NTU)$	0.1394	0.0492	0.3840	0.4589	0.3790	0.3945

Considering Table 3, it could be concluded that the BLR model is one of the reliable models with lower computational costs that can be used for water quality parameters' prediction in the Gorgan Gulf using Sentinel-2. The RMSE of the model in each date (RMSE (1)) in both dates for all of the parameters is lower than 0.5. On the other hand, the comparison between the RMSE (1) at 28 June 2021 and the RMSE of the predicted water quality parameters at 28 June 2021 by the model created for the 11 September 2020 (RMSE (2)) illustrates that although the RMSE increases, the model still is a valuable predictor because the RMSE (2) is lower than 1 for all of the parameters. The comparison between RMSE (2) for the model with seven bands and RMSE (2) for the model with four bands indicates that using four bands not only reduces computational costs because of the fewer inputs but also decreases RMSE (2). This means that the model with four bands could be a better predictor than the model with seven bands.

4.3. Exported Maps of the BLR Model

Exported maps based on the BLR model of each date are presented in Figure 5. these maps are exported using four bands input employing GEE.

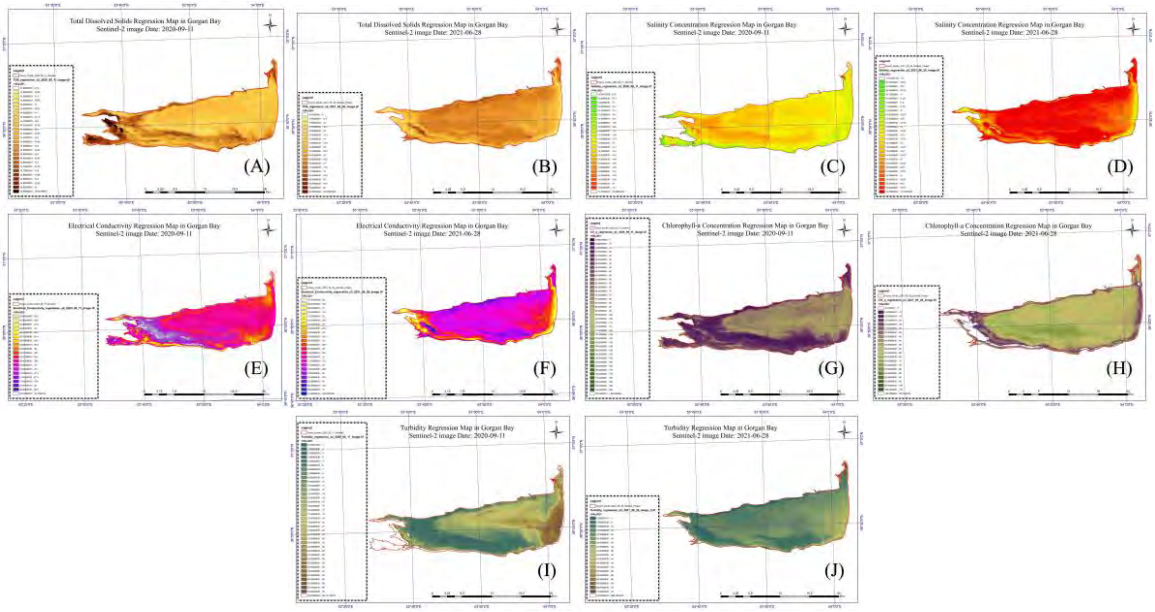

Figure 5: Exported Gorgan Gulf water quality parameters maps using BLR model with four bands input. These maps are exported for 11 September 2020 for (A) TDS, (C) Salinity, (E) EC, (G) Chl-a, (I) Turbidity, and 28 June 2021 for (B) TDS, (D) Salinity, (F) EC, (H) Chl-a, and (I) Turbidity.

5. CONCLUSIONS

This study shows the importance of band selection for water quality parameters. To this end, five water quality parameters (TDS, Salinity, EC, Chl-a, and Turbidity) in Gorgan Gulf were predicted using field measured data on 11 September 2020 and 28 June 2021 and data Sentinel-2 satellite data. A BLR model with two series of bands (seven bands: Aerosols, Blue, Green, Red, NIR, SWIR1, SWIR2, and four bands: Blue, Green, Red, NIR) was used to predict the water quality parameters.
Results indicate that using four bands is more rational because it covers the wavelength range of water spectral signature, reduces computational costs, and gives better RMSE than seven bands. Also, results show that the BLR model could be a reasonable model for Gorgan Gulf water quality parameters' prediction using Sentinel-2 satellite because the model prediction RMSE is lower than 1 for all the parameters.

6. ACKNOWLEDGMENT

Authors express their appreciation to Mohamadreza Kanani and Hosseinali Ebrahimi, members of the Department of Environment Islamic Republic of Iran (DOE), for their support in collecting field data.

7. REFERENCES

[1] N. Torbick, S. Hession, S. Hagen, N. Wiangwang, B. Becker, and J. Qi, “Mapping inland lake water quality across the Lower Peninsula of Michigan using Landsat TM imagery,” *International Journal of Remote Sensing*, vol. 34, no. 21, pp. 7607–7624, Nov. 2013, doi: 10.1080/01431161.2013.822602.
[2] J. Bartram, R. Ballance, United Nations, and World Health Organization, Eds., *Water quality monitoring: a practical guide to the design and implementation of freshwater quality studies and monitoring programmes*, 1st ed. London ; New York: E & FN Spon, 1996.
[3] “Report of the 18th Session of GESAMP, 1988,” *GESAMP*. http://www.gesamp.org/publications/report-of-the-18th-session (accessed 24 July, 2020).
[4] “reviving-the-dead-zone.pdf.”
[5] E. Hazen, J. Craig, C. Good, and L. Crowder, “Vertical distribution of fish biomass in hypoxic waters on the Gulf of Mexico shelf,” *Mar. Ecol. Prog. Ser.*, vol. 375, pp. 195–207, Jan. 2009, doi: 10.3354/meps07791.

[6] P. A. Brivio, C. Giardino, and E. Zilioli, "Validation of satellite data for quality assurance in lake monitoring applications," *Science of The Total Environment*, vol. 268, no. 1–3, pp. 3–18, Mar. 2001, doi: 10.1016/S0048-9697(00)00693-8.
[7] J. W. Chipman *et al.*, *Remote sensing methods for lake management: a guide for resource managers and decision-makers*. Madison, WI: North American Lake Management Society, 2009.
[8] A. Bhatti, S. Nasu, M. Takagi, and Y. Nojiri, "Assessing the potential of remotely sensed data for water quality monitoring of coastal and inland waters," *Res. Bull. Kochi Univ. Technol.*, vol. 5, Jan. 2008.
[9] K. D. Haddad, B. A. Harris, and International Symposium on Machine Processing of Remotely Sensed Data, Eds., *Assessment and trends of Florida's marine fisheries habitat: an integration of aerial photography and thematic mapper imagery*. West Lafayette, Ind.: Laboratory for Applications of Remote Sensing, Purdue University, 1985.
[10] F. Mushtaq and M. G. Nee Lala, "Remote estimation of water quality parameters of Himalayan lake (Kashmir) using Landsat 8 OLI imagery," *Geocarto International*, vol. 32, no. 3, pp. 274–285, Mar. 2017, doi: 10.1080/10106049.2016.1140818.
[11] Y. H. Kim, J. Im, H. K. Ha, J.-K. Choi, and S. Ha, "Machine learning approaches to coastal water quality monitoring using GOCI satellite data," *GIScience & Remote Sensing*, vol. 51, no. 2, pp. 158–174, Mar. 2014, doi: 10.1080/15481603.2014.900983.
[12] E. Siswanto *et al.*, "Empirical ocean-color algorithms to retrieve chlorophyll-a, total suspended matter, and colored dissolved organic matter absorption coefficient in the Yellow and East China Seas," *J Oceanogr*, vol. 67, no. 5, pp. 627–650, Oct. 2011, doi: 10.1007/s10872-011-0062-z.
[13] E. T. Harvey, S. Kratzer, and P. Philipson, "Satellite-based water quality monitoring for improved spatial and temporal retrieval of chlorophyll-a in coastal waters," *Remote Sensing of Environment*, vol. 158, pp. 417–430, Mar. 2015, doi: 10.1016/j.rse.2014.11.017.
[14] M. Bayati and M. Danesh-Yazdi, "Mapping the spatiotemporal variability of salinity in the hypersaline Lake Urmia using Sentinel-2 and Landsat-8 imagery," *Journal of Hydrology*, vol. 595, p. 126032, Apr. 2021, doi: 10.1016/j.jhydrol.2021.126032.
[15] G. Sent *et al.*, "Deriving Water Quality Parameters Using Sentinel-2 Imagery: A Case Study in the Sado Estuary, Portugal," *Remote Sensing*, vol. 13, no. 5, p. 1043, Mar. 2021, doi: 10.3390/rs13051043.
[16] R. Katlane, C. Dupouy, B. E. Kilani, and J. C. Berges, "Estimation of Chlorophyll and Turbidity Using Sentinel 2A and EO1 Data in Kneiss Archipelago Gulf of Gabes, Tunisia," *IJG*, vol. 11, no. 10, pp. 708–728, 2020, doi: 10.4236/ijg.2020.1110035.
[17] K. A. Kilpatrick *et al.*, "A decade of sea surface temperature from MODIS," *Remote Sensing of Environment*, vol. 165, pp. 27–41, Aug. 2015, doi: 10.1016/j.rse.2015.04.023.
[18] M. Kabolizadeh, K. Rangzan, S. Zareie, M. Rashidian, and H. Delfan, "Evaluating quality of surface water resources by ANN and ANFIS networks using Sentinel-2 satellite data," *Earth Sci Inform*, Jan. 2022, doi: 10.1007/s12145-021-00741-z.
[19] F. M. C. Pizani, P. Maillard, A. F. F. Ferreira, and C. C. de Amorim, "ESTIMATION OF WATER QUALITY IN A RESERVOIR FROM SENTINEL-2 MSI AND LANDSAT-8 OLI SENSORS," *ISPRS Ann. Photogramm. Remote Sens. Spatial Inf. Sci.*, vol. V-3–2020, pp. 401–408, Aug. 2020, doi: 10.5194/isprs-annals-V-3-2020-401-2020.
[20] "Sentinel-2 MSI: MultiSpectral Instrument, Level-2A | Earth Engine Data Catalog," *Google Developers*. https://developers.google.com/earth-engine/datasets/catalog/COPERNICUS_S2_SR (accessed 09 January, 2022).
[21] T. J. Mitchell and J. J. Beauchamp, "Bayesian Variable Selection in Linear Regression," *Journal of the American Statistical Association*, vol. 83, no. 404, pp. 1023–1032, Dec. 1988, doi: 10.1080/01621459.1988.10478694.
[22] M. Mahsuli, "Probabilistic models, methods, and software for evaluating risk to civil infrastructure," University of British Columbia, 2012. doi: 10.14288/1.0050878.
[23] H. Nasrazadani and M. Mahsuli, "Probabilistic Framework for Evaluating Community Resilience: Integration of Risk Models and Agent-Based Simulation," *J. Struct. Eng.*, vol. 146, no. 11, p. 04020250, Nov. 2020, doi: 10.1061/(ASCE)ST.1943-541X.0002810.
[24] M. Mahsuli and T. Haukaas, "Computer Program for Multimodel Reliability and Optimization Analysis," *J. Comput. Civ. Eng.*, vol. 27, no. 1, pp. 87–98, Jan. 2013, doi: 10.1061/(ASCE)CP.1943-5487.0000204.
[25] P. Onjira, "Application of Remote sensing and Rainfall-Run-off Inundation Modeling to Near-Real Time Flood Monitoring in Kenya," 2014. doi: 10.13140/RG.2.1.1283.3046.